MINERAL CO_2 SEQUESTRATION IN INDUSTRIAL WASTE MATERIALS: A COMPARATIVE STUDY USING FTIR, TGA AND CALCIMETRY

SARA TOMINC,[1] MAJDA PAVLIN,[1] MARUŠA MRAK,[1] VILMA DUCMAN,[1] OGNJEN RUDIĆ,[2,3] CYRILL GRENGG[2]

[1] Slovenian National Building and Civil Engineering Institute, Ljubljana, Slovenia
sara.tominc@zag.si, majda.pavlin@zag.si, marusa.mrak@zag.si, vilma.ducman@zag.si
[2] Graz University of Technology, Institute of Applied Geosciences, Graz, Austria
ognjen.rudic@tugraz.at, cyrill.grengg@tugraz.at
[3] Graz University of Technology, Institute of Technology and Testing of Building Materials, Graz, Austria
ognjen.rudic@tugraz.at

Mineral CO_2 sequestration is a promising approach for reducing greenhouse gas emissions by storing CO_2 in stable forms permanently. This process involves capturing CO_2 and converting it into solid carbonates through mineralisation. Waste ashes and slags, by-products of waste incineration and steel production, are promising materials for CO_2 sequestration, due to their high alkalinity and reactive mineral phases. In this study, the CO_2 sequestration potentials of different metallurgical slags and incineration ashes from Austria and Slovenia were analysed using Fourier transform infrared spectroscopy (FTIR), thermogravimetric analysis (TGA), and calcimetry. Biomass ash (A1) showed the highest sequestration capacity of 153.7 g CO_2 per kg of ash.

DOI
https://doi.org/10.18690/um.fkkt.1.2026.8

ISBN
978-961-299-130-2

Keywords:
CO_2 sequestration capacity, enhanced carbonation, thermogravimetric analysis, calcimetry, Fourier transform infrared spectroscopy

University of Maribor Press

1 Introduction

CO_2 is the most significant greenhouse gas (GHG) produced by human activities, accounting for about two-thirds of the enhanced greenhouse effect. The development of carbon capture and storage (CCS) technologies is one possible strategy to reduce atmospheric CO_2 (Medas et al., 2017). Mineral CO_2 sequestration is a carbon capture and storage process in which CO_2 reacts chemically with Ca- and Mg-containing minerals to form stable carbonate products (Li and Wu, 2022). Alkaline residues such as slags and ashes typically contain highly reactive Ca and Mg species that are potentially suitable for high and rapid carbonate conversion without the need for pre-treatment or energy-intensive operating conditions (Medas et al., 2017, Alturki, 2022; Li and Wu, 2022). For the steel industry, responsible for almost 8% of global CO_2 emissions, mineral carbonation technologies present a major opportunity, as the mineralisation of iron and steel slags could reduce its carbon footprint directly. Consequently, integrating carbon capture and storage management into the circular economy framework is crucial for progress towards global environmental goals (Capelo-Avilés et al., 2024).

Enhanced carbonation treatment has recently been developed extensively to improve the capacity and efficiency of CO_2 sequestration. Compared to natural carbonation, enhanced carbonation increases both the reaction rate and the carbon storage potential of materials significantly. Based on the exposure conditions applied during the CO_2 mineralisation process, carbonation treatments are generally divided into three main categories: gas-solid carbonation (dry carbonation), semi-dry carbonation (with water vapour), and aqueous carbonation (in suspension) (Li and Wu, 2022, Zajac et al., 2022). In the aqueous phase, the main mineralisation reaction involves the initial hydration of the free Ca and Mg oxides to form Ca and Mg hydroxides, followed by carbonation to Ca and Mg carbonates (Capelo-Avilés et al., 2024). Several factors influence the rate and extent of carbonation, including the CO_2 partial pressure, temperature and moisture or water content. Carbonation is enhanced by the addition of water or moisture, which promotes CO_2 dissolution and leaching of Ca^{2+} from the mineral constituents, while excessive water can hinder CO_2 diffusion by blocking the pores of the matrix. The reaction rate can also be increased by raising the temperature to between 30 and 60 °C. However, carbonation efficiency decreases above 60 °C due to the lower solubility of CO_2 in water at higher temperatures (Ukwattage et al., 2015).

In addition, carbonated mineral residues can be used in the production of construction materials (cement and concrete, road construction, lightweight aggregates and AAMs), wastewater treatment, or environmental remediation. For example, carbonated slag has significant potential for the cement industry, as the carbonation process can improve the hydraulic properties of this by-product (Biava et al., 2024). In this study, the CO_2 sequestration potential of selected industrial residues from Austria and Slovenia was evaluated, with the aim of using the resulting carbonated mineral residues as secondary raw materials for the production of sustainable mineral-based construction materials.

2 Materials and methods

Two types of raw materials were selected for this study: waste ash and slag. The ash samples were wood biomass bottom ash (A1) and coal fly ash with added bauxite (A2), while the slag samples were electric arc furnace (EAF) slag (S1) and a mixture of electric arc furnace stainless (EAF-S) slag and ladle slag (S2).

Before the chemical analysis the samples were dried in a laboratory oven at 105 °C to a constant weight and sieved to a particle size below 125 µm. To determine the loss on ignition (LOI), the samples were heated at 950 °C in accordance with EN 196-2:2013. The fused beads were prepared by mixing ash with a flux of 50% lithium tetraborate and 50% lithium metaborate at a ratio of 1:10 (0.947 g ash to 9.47 g flux) and heating at 1100 °C. The chemical composition of the samples was analysed using a Thermo Scientific ARL PERFORM'X Wavelength Dispersive X-ray Fluorescence Spectrometer (WDXRF) equipped with an Rh-target X-ray tube and UniQuant software.

For the mineralogical analysis, each sample was sieved to below 63 µm and placed in 27 mm diameter holders. To minimise the effects of the preferred orientation, the samples were back-loaded into a circular sample holder. An X-ray diffraction (XRD) analysis was performed before and after carbonation using a PANalytical Empyrean X-ray diffractometer with a CuKα1 X-ray source. The X-ray tube was operated at 45 kV and 40 mA. The measurements were carried out in a 2θ range of 4-70° with a step size of 0.013° 2θ. The external standard method with corundum (NIST SRM 676a) was used to determine the amorphous phase. The quantitative phase analysis was performed using XRD powder patterns and ICDD PDF-4 (2020) database files,

applying Rietveld refinement with the PANalytical X'Pert HighScore Plus diffraction software (version 4.9).

The sequestration potential of 15 g of each sample with a particle size below 125 μm was tested using a modified method (Tominc and Ducman, 2023) for semi-dry carbonation at a controlled relative humidity of 80 ± 3.2 %, a temperature of 40 ± 0.5 °C, and a CO_2 concentration of 20 ± 0.1 vol% for 72 hours. Before exposure in the carbonation chamber, the samples were mixed with 10 wt.% water. Carbonation was considered complete when a constant mass was reached. The CO_2 content (wt.%) in the samples was determined by FTIR, TGA and calcimeter, and the CO_2 uptake was calculated based on Equation (1) (Medas et al., 2017, Nielsen and Quaghebeur, 2023):

$$CO_{2\ uptake}(wt\%) = \frac{(CO_{2\ carb}\ (wt\%) - CO_{2\ orig}\ (wt\%))}{(100 - CO_{2\ carb}\ (wt\%))} \times 100 \quad (1)$$

The CO_2 uptake quantifies the increase in CO_2 content during the carbonation process, while the CO_2 sequestration capacity ($CO_{2\ capacity}$) indicates the total amount of CO_2 that can be sequestered per kilogram of the analysed sample (g_{CO2}/kg_{sample}). The CO_2 sequestration capacity of each sample was calculated using Equation (2) (Capelo-Avilés et al., 2024). $CO_{2\ carb}$ refers to the measured CO_2 content in the sample (wt%) after complete carbonation.

$$CO_{2\ capacity}(g_{CO2}/kg_{sample}) = \frac{CO_{2\ carb}\ (wt\%)}{100 - CO_{2\ carb}\ (wt\%)} \times 1000 \quad (2)$$

For the calcimetry, which measures the carbonate content based on its reaction with 10% hydrochloric acid, the CO_2 release was measured using a pressure calcimeter (OFITE Calcimeter, OFI Testing Equipment Inc., USA, according to ASTM D 4373) with an analytical error below 5%. The calcimeter was calibrated before the measurements by reacting HCl with a $CaCO_3$ standard (Calcium Carbonate Precipitated, OFI Testing Equipment, Inc., CAS: 471-34-1). The calibration curve (Figure 1) was generated from five measurements (0.2, 0.4, 0.6, 0.8, and 1.0 g $CaCO_3$) with R^2=0.9996.

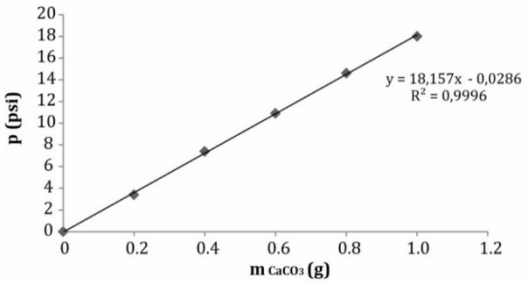

Figure 1: Calibration curve for the calcimetric measurements.
Source: own.

Thermogravimetric analysis (TGA) was performed on dry samples using a TGA Q5000IR thermal analyser (TA Instruments, New Castle, Delaware, USA). The analysis followed a controlled heating programme with a ramp rate of 10 K min^{-1} from 25 to 1000 °C. To prevent oxidation, the sample chamber was filled with N_2 at a flow rate of 25 mL min^{-1}. Approximately 20 mg of each sample was placed in 100 µL Al_2O_3 crucibles. The CO_2 content was determined from the mass loss within the temperature range associated with the decomposition of the carbonate mineral (500-800 °C), based on the dry matter at 105 °C (Capelo-Avilés et al., 2024). The measurements were analysed using a TA Universal Analysis 2000 v.4.5A (TA Instruments, New Castle, Delaware, USA). Each sample was tested individually.

A Fourier transform infrared (FTIR) spectrometer (PerkinElmer Spectrum Two, Kentucky, USA) equipped with an attenuated total reflection accessory (Universal ATR) was used to observe the infrared spectra of the analysed samples, using a diamond crystal as a solid sample support, in the range 380-4000 cm^{-1} at a resolution of 4 cm^{-1}. The standards calcite (Calcium Carbonate Precipitated, OFI Testing Equipment, Inc., CAS: 471-34-1) and quartz (Silicon Dioxide, Sigma-Aldrich, Co., CAS:60676-86-0) with known concentrations were used to generate a calibration curve (Figure 2). The calibration curve was generated with eight measurements (100% SiO_2, 95% SiO_2 + 5% $CaCO_3$, 90% SiO_2 + 10% $CaCO_3$, 80% SiO_2 + 20% $CaCO_3$, 70% SiO_2 + 30% $CaCO_3$, 50% SiO_2 + 50% $CaCO_3$, 30% SiO_2 + 70% $CaCO_3$ and 100% $CaCO_3$), with a correlation of 0.9993 and a standard error of 1.47%. After the spectra were acquired for ATR-FTIR, automatic baseline correction was performed, and the positions and peak heights were recorded using the Spectrum Quant 10.6 software.

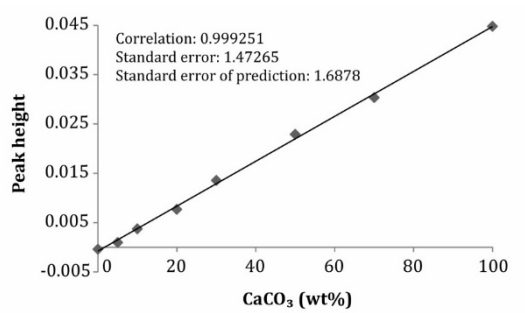

Figure 2: Calibration curve for FTIR.
Source: own.

3 Results and Discussion

The X-ray fluorescence analysis (XRF) revealed that the untreated analysed ashes and slags are composed mainly of CaO (18-37%), SiO_2 (11-39%) and Al_2O_3 (7-32%), with varying amounts of MgO (1-13%), Fe_2O_3 (0-33%), SO_3 (0.1-4%) and K_2O (0.01-3%), while Na_2O was present only in low concentrations. Of these, the contents of CaO and MgO are of particular interest, as these oxides play a key role in mineral carbonation. Both react with CO_2 to form stable carbonates, making these residues promising candidates for CO_2 sequestration. Among the analysed samples, A1 and S2, which have the highest CaO and MgO contents, show high potential for carbonation and, consequently, significant CO_2 uptake. The detailed chemical composition and the LOI at 950 °C are presented in Table 1.

The carbonation behaviour of the samples was investigated under controlled conditions. The reaction was completed after 72 hours, and the reaction rate was increased significantly by the addition of 10 wt.% water and a higher CO_2 concentration compared to our previous study (Tominc and Ducman, 2025), in which 4 vol.% CO_2 was used without water added before placing the samples in the carbonation chamber. The literature also indicates that the presence of water plays a crucial role in enhanced carbonation, as it allows the dissolution of CO_2, promotes the formation of bicarbonate/carbonate ions, increases the mobility of Ca^{2+} and Mg^{2+}, and provides the medium for the nucleation and precipitation of stable carbonates (Medas et al., 2017, Capelo-Avilés et al., 2024).

Table 1: Chemical composition of the analysed ashes and slags in terms of primary oxides (wt.%), measured by XRF, and LOI at 950 °C.

Sample ID	LOI $_{950\ °C}$	Al_2O_3	SiO_2	CaO	MgO	Fe_2O_3	K_2O	Na_2O	SO_3
A1	9.38	7.28	39.0	29.35	4.56	3.42	3.01	1.02	0.76
A2	23.39	32.08	10.87	17.71	0.64	6.40	2.21	0.41	4.09
S1	0.20	14.33	13.82	22.91	6.32	32.96	0.01	0.35	0.11
S2	9.60	9.58	18.16	37.41	13.49	7.55	0.01	0.00	0.29

Source: own

A comparison of the untreated and carbonated samples highlights the effect of carbonation on their mineralogical composition. As shown in Table 2 and Figure 3, phases susceptible to carbonation decreased progressively, indicating their transformation into carbonation products.

Table 2: Phase composition of the analysed ashes and slags (wt.%).

Mineral	Formula	A1 untr	A1 carb	A2 untr	A2 carb	S1 untr	S1 carb	S2 untr	S2 carb
calcite	$CaCO_3$	9.7	19.9	19.5	23.8	1.3	5.2	7.6	10.7
portlandite	$Ca(OH)_2$	12.5	0.5	-	-	-	-	-	-
ettringite	$Ca_6Al_2(SO_4)_3(OH)_{12}\cdot 26H_2O$			8.7	0.7				
gamma belite	γ-Ca_2SiO_4	-	-	-	-	12.8	2.7	5.3	4.1
gehlenite	$Ca_2Al_2SiO_7$	-	-	24.0	24.3	-	-	-	-
wüstite	FeO	-	-	16.1	16.3	-	-	-	-
quartz	SiO_2	7.8	8.4	1.0	1.2	-	-	-	-
akermanite	$Ca_2Mg(Si_2O_7)$	10.0	9.4	-	-	-	-	-	-
magnetite	Fe_3O_4	-	-	6.1	5.9	-	-	-	-
anhydrite	$CaSO_4$	-	-	5.5	5.4	-	-	-	-
periclase	MgO	-	-	-	-	-	-	4.7	4.2
diaspore	AlO(OH)	-	-	3.7	4.4	-	-	-	-
anorthite	$CaAl_2Si_2O_8$	-	-	3.1	3.2	-	-	-	-
gypsum	$CaSO_4\cdot 2H_2O$	-	-	3.0	0.0	-	-	-	-
merwinite	$Ca_3Mg(SiO_4)_2$	-	-	-	-	-	-	2.0	1.9
hematite	Fe_2O_3	-	-	1.4	2.0	-	-	-	-
brucite	$Mg(OH)_2$	-	-	-	-	-	-	<1.0	<1.0
ACn*		60.0	61.8	54.1	59.3	39.7	45.6	66.1	68.6

*ACn : Amorphous and Crystalline non-quantifiable phases; untr: untreated
Source: own

In the untreated A1 sample, the main crystalline phases were calcite (9.7 wt.%), portlandite (12.5 wt.%), akermanite (10.0 wt.%) and quartz (7.8 wt.%). After CO_2 treatment, a significant change in the mineral composition was observed, as the portlandite reacted (0.5 wt.%) with CO_2 almost completely to form calcite (19.9 wt.%). The phase assemblage of the untreated A2 sample contained mainly calcite,

ettringite and anhydrite, with low quantities of gypsum, hematite, diaspore, anorthite and quartz. The sample showed only a slight increase in calcite content (from 19.5 to 23.8 wt.%), suggesting a high degree of carbonation already during storage. However, during carbonation, the CO_2 reacts with the Ca-bearing phases such as ettringite (decreasing from 8.7 to 0.7 wt.%), leading to their decomposition and likely resulting in the formation of calcite and amorphous or poorly crystalline phases. The sulphate phases, such as gypsum and anhydrite, also decreased, while the inert minerals, such as hematite, diaspore and quartz showed little to no reaction. Meanwhile, the ACn fraction increased from 54.1 to 59.3 wt.%, which aligns with the formation of amorphous carbonation products following the breakdown of the ettringite and other Ca-bearing phases. The original sample S1 contained calcite, gamma belite, gehlenite, magnetite and wüstite. During carbonation, the gamma belite reduced noticeably (from 12.8 to 2.7 wt.%), indicating an extensive reaction with CO_2, consistent with the increase in calcite content (from 1.3 to 5.2 wt.%). Gehlenite, magnetite and wüstite are mostly inert under normal carbonation conditions. The ACn fraction increased from 39.7 to 45.6 wt.%, further supporting the formation of non-crystalline carbonation products. In sample S2, the calcite formation became increasingly prominent, rising from 7.6 to 10.7 wt.%, confirming calcite as the main carbonation product. The Ca- containing phases such as gamma belite react readily with CO_2 to form calcite (Chen et al., 2021). In the presence of water and CO_2, γ-belite and any residual β-belite can undergo carbonation, generating C-S-H and calcite (Chang et al., 2016). Other Ca-rich phases, including merwinite, showed lower carbonation reactivity.

Overall, Table 2 shows clearly that carbonation increased the calcite content in all the samples and decreased the carbonatable phases such as portlandite, ettringite and γ-belite. In contrast, phases such as gehlenite, magnetite, wüstite, anhydrite and quartz remained largely inert under the tested conditions.

For TGA, the mass loss between 500 and 800 °C was attributed to the thermal decomposition of $CaCO_3$ into CaO and CO_2 (Figure 4), while the mass loss at lower temperatures was attributed to the removal of organic carbon (typically in the range 250-500 °C), partial decomposition of the portlandite (usually around 400 °C, as shown in Figure 4a (the orange dotted lines), or the decomposition of the aluminate-ferrite-monosulphate (AFm) phases (such as monosulphate, monocarbonate, or Friedel's salt). This was distinctive for sample S2, and is recognisable as mass loss at around 140 and 400 °C (as shown in Figure 4b).

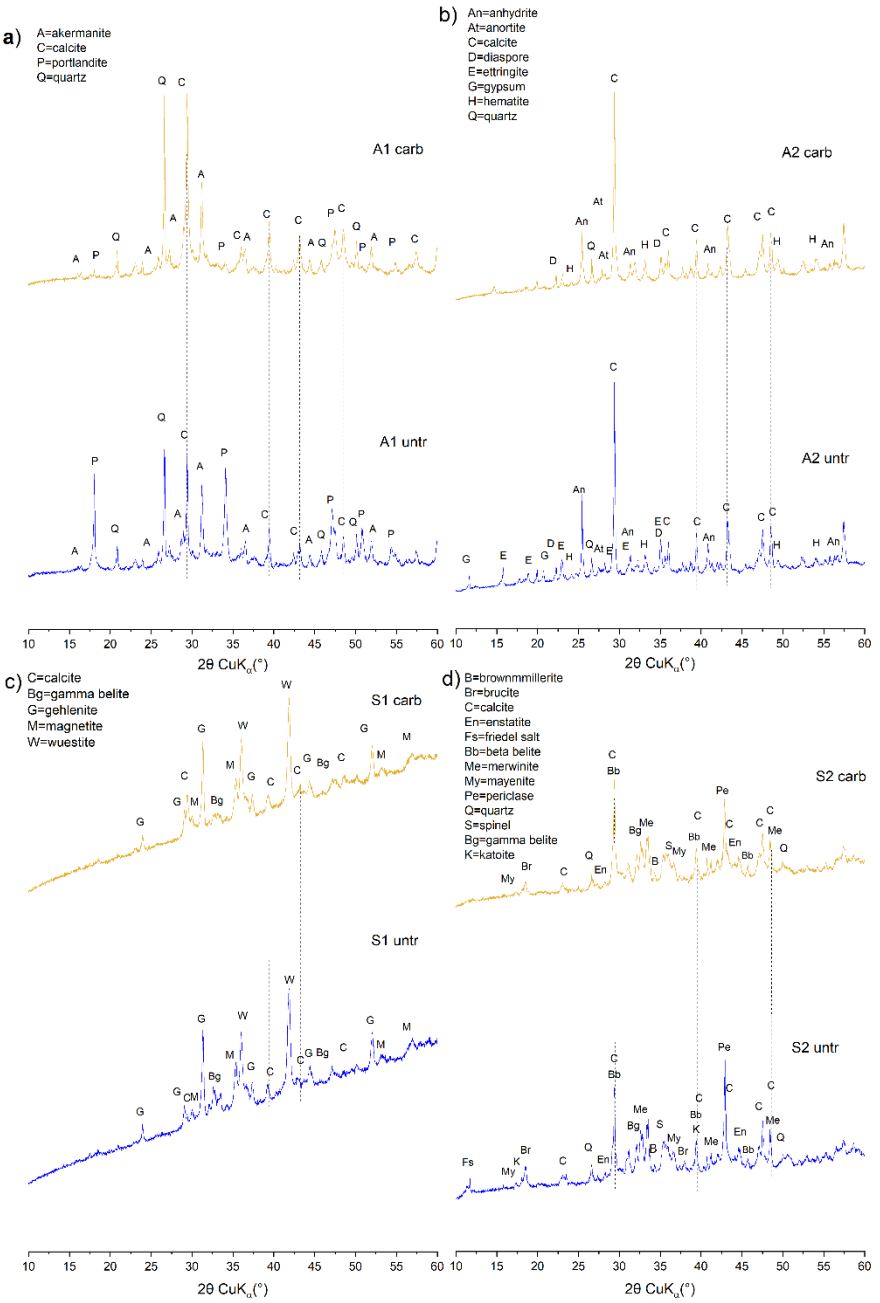

Figure 3: X-ray diffraction patterns of the untreated and carbonated samples: a) A1, b) A2, c) S1, and d) S2. Calcite, the main carbonation product, is indicated by the dotted lines.

Source: own.

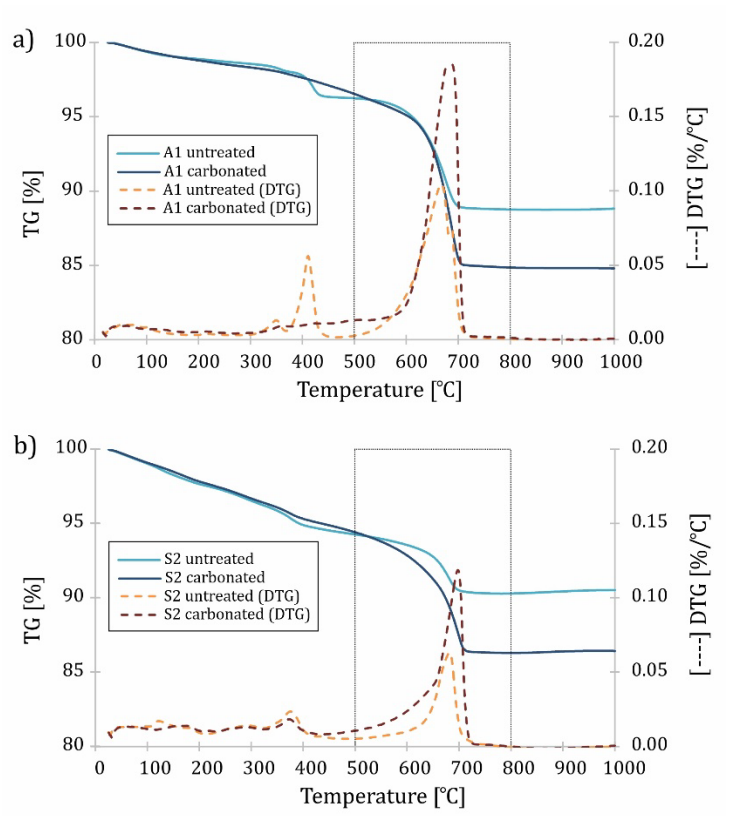

Figure 4: TG/DTG curves of the selected samples after 72 hours of carbonation for a) A1 and b) S2, showing the maximum CO_2 content in the temperature range 500-800 °C.

Source: own.

The FTIR analysis, which estimates the $CaCO_3$ content based on characteristic absorption bands, showed trends consistent with those of TGA, with only minor deviations observed at low levels of carbonation (e.g., S1 original). The FTIR spectra of the carbonated samples (Figure 5) showed the characteristic C-O bonds typical of carbonate phases, with a strong band at approximately 1410 cm^{-1} corresponding to the ν_3 vibrations of CO_3^{2-} (asymmetric C-O stretching). Additional bands at around 874 cm^{-1} and 712 cm^{-1} are attributed to the ν_2 out of-plane and in-plane bending vibrations of CO_3^{2-} from the trace carbonate compounds (Capelo-Avilés et al., 2024). The increased intensity of these bands in the carbonated samples confirms the formation of $CaCO_3$ during carbonation, consistent with the TGA and

calcimetric measurements. For the calcimetric measurements, the CO_2 content of the samples was determined using the stoichiometric ratios given in Equation (3):

$$CaCO_3 + 2HCl \rightarrow CaCl_2 + CO_2 + H_2O \quad (3)$$

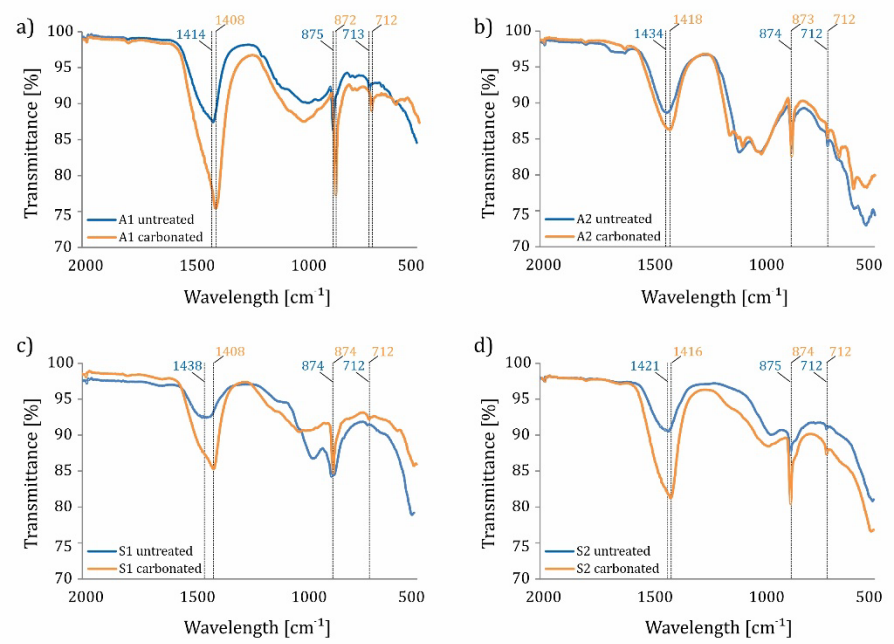

Figure 5: FTIR spectra of samples a) A1, b) A2, c) S1 and d) S2.
Source: own.

Table 3: Comparative analysis of $CaCO_3$ and CO_2 content before and after enhanced carbonation, determined by TGA, pressure calcimeter and quantitative FTIR.

Sample ID		TGA		FTIR		Calcimeter	
		CO_2/dry matter (wt%)	$CaCO_3$ (wt%)	CO_2 (wt%)	$CaCO_3$ (wt%)	CO_2 (wt%)	$CaCO_3$ (wt%)
A1	untr	7.6	**17.2**	7.6	**17.3**	5.5	**12.4**
	carb	11.8	**26.8**	12.8	**29.1**	13.3	**30.3**
A2	untr	9.8	**22.2**	10.5	**23.8**	10.8	**24.6**
	carb	10.8	**24.4**	11.8	**26.8**	11.2	**25.4**
S1	untr	0.9	**2.0**	2.6	**5.8**	2.2	**4.9**
	carb	3.2	**7.3**	3.6	**8.3**	5.3	**12.1**
S2	untr	4.0	**9.2**	4.1	**9.3**	4.1	**9.4**
	carb	8.2	**18.6**	8.1	**18.5**	9.8	**22.3**

Source: own

A comparative assessment of the $CaCO_3$ content before and after accelerated carbonation was performed using TGA, calcimetry and quantitative FTIR. All three techniques provided consistent estimates of the CO_2 content, with differences of less than 3 wt.%, as shown in Table 3.

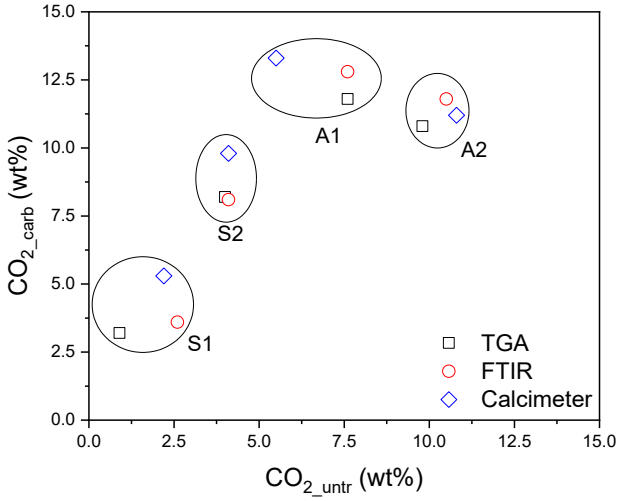

Figure 6: Comparison of the calculated CO_2 content (wt.%) before and after carbonation, determined by three analytical methods (TGA, FTIR and calcimeter). The scatter plot shows good agreement between the analytical methods for each sample.

Source: own.

The CO_2 uptake was calculated according to Equation (1). For most samples, the pressure calcimeter gives higher CO_2 uptake and capacity values than TGA and FTIR. The main limitation of TGA is the possible overlap in decomposition temperatures, while, for FTIR, weak peaks and peak overlap are also major limitations. The pressure calcimeter provides a more realistic estimate of the maximum capacity. Among the samples tested, biomass ash A1 showed the greatest increase in $CaCO_3$ content after CO_2 exposure, corresponding to a CO_2 uptake of 9.1 wt.% and CO_2 sequestration capacity of 153.7 g CO_2 per kg of ash according to the calcimetric measurements (Table 4). In contrast, ash A2 was found to be almost completely carbonated during storage, indicating high reactivity even under ambient conditions. The CO_2 uptake in ash A2 was only 0.4 wt.%; however, the CO_2 sequestration capacity was 125.7 g CO_2 per kg of ash. Sample S2, with a CO_2 uptake of 6.3 wt.%, demonstrated considerable potential for CO_2 sequestration, with a

capacity of 108.7 g CO_2 per kg of slag, while sample S1, with a CO_2 uptake of 3.3 wt.%, showed a comparatively lower carbonation potential, with a capacity of 56.2 g CO_2 per kg of slag, due to a lower proportion of reactive Ca- and Mg-containing minerals.

Table 4: CO_2 uptake (wt.%) and CO_2 sequestration capacity (g_{CO2}/kg_{sample}) of the analysed samples determined by TGA, FTIR and calcimeter.

Sample ID	TGA		FTIR		Calcimeter	
	CO_2 uptake	CO_2 capacity	CO_2 uptake	CO_2 capacity	CO_2 uptake	CO_2 capacity
A1	4.8	133.4	5.9	146.7	9.1	153.7
A2	1.1	120.5	1.5	133.6	0.4	125.7
S1	2.4	33.3	1.1	37.9	3.3	56.2
S2	4.5	89.1	4.4	88.6	6.3	108.7

Source: own

4 Conclusions

The potential for CO_2 sequestration in wood biomass bottom ash (A1), coal fly ash with added bauxite (A2), EAF slag (S1), and a mixture of EAF stainless slag and ladle slag (S2) was assessed, to support ongoing research aimed at reducing the carbon footprint of industrial processes. The selected waste materials have the potential for permanent CO_2 binding, with sequestration capacities of 56.2-153.7 g CO_2 per kg of sample according to the calcimetric measurements. In addition, the analysed materials will be used further as feedstock for the development of mineral-based construction materials, thus offering significant potential for applications in construction, infrastructure and environmental technology.

Acknowledgment

This work was supported by the Slovenian Research Agency and the Austrian Science Fund under Project no. N2-0320/I 6481-N (Waste to alkali-activated binders (WIN)), and was supported partially by the Slovenian Research and Innovation Agency (ARIS) under Research Core Grant no. P2-0273.

Data availability status

The original data presented in the study are openly available in the DiRROS repository at the following link: http://hdl.handle.net/20.500.12556/DiRROS-24534.

References

Alturki, A. (2022). The Global Carbon Footprint and How New Carbon Mineralization Technologies Can Be Used to Reduce CO_2 Emissions. *ChemEngineering, 6*, 44. doi:10.3390/chemengineering6030044

Biava, G., Depero, L.E., Bontempi E. (2024). Accelerated Carbonation of Steel Slag and Their Valorisation in Cement Products: A Review. *Spanish Journal of Soil Science, 14*,12908. doi: 10.3389/sjss.2024.12908

Capelo-Avilés, S., Tomazini de Oliveira, R., Gallo Stampino, I.I., Gispert-Guirado, F., Casals-Terré, A., Giancola, S., Galán-Mascarós, J.R. (2024). A thorough assessment of mineral carbonation of steel slag and refractory waste. *Journal of CO_2 Utilization, 82*, 102770. doi:10.1016/j.jcou.2024.102770

Chang, J., Fang, Y., Shang, X. (2016). The role of β-C_2S and γ-C_2S in carbon capture and strength development. *Materials and Structures, 49*, 4417–4424. doi:10.1617/s11527-016-0797-5

Chen, Z., Cang, Z., Yang, F., Zhang, J., Zhang, L. (2021). Carbonation of steelmaking slag presents an opportunity for carbon neutral: A review. *Journal of CO_2 Utilization, 54*, 101738. doi:10.1016/j.jcou.2021.101738

Li, L., Wu, M. (2022). An overview of utilizing CO_2 for accelerated carbonation treatment in the concrete industry. *Journal of CO_2 Utilization, 60*, 102000. doi:10.1016/j.jcou.2022.102000

Medas, D.,Cappai, G., De Giudici, G., Piredda, M. and Podda, S. (2017). Accelerated carbonation by cement kiln dust in aqueous slurries: chemical and mineralogical investigation. *Greenhouse Gasses: Science and Technology,7(4)*, 692–705. doi: 10.1002/ghg.1681

Nielsen, P., Quaghebeur, M. (2023). Determination of the CO_2 Uptake of Construction Products Manufactured by Mineral Carbonation. *Minerals, 13*, 1079. doi:10.3390/min13081079

Scrivener, K., Snellings, R. Lothenbach, B. (Eds.). (2016). A Practical Guide to Microstructural Analysis of Cementitious Materials (1st ed.). CRC Press. doi:10.1201/b19074

Tominc, S., Ducman, V. (2023). Methodology for Evaluating the CO_2 Sequestration Capacity of Waste Ashes. *Materials, 16*, 5284. doi:10.3390/ma16155284

Tominc, S., Ducman, V. (2025). Determination of the maximum CO_2 sequestration capacity of Slovenian waste ashes using thermogravimetry and calcimetry. *7th International Conference on Technologies & Business Models for Circular Economy: Conference Proceedings, 7*, 151-159. doi:10.18690/um.fkkt.1.2025.13

Ukwattage, N.L., Ranjith, P.G., Yellishetty, M. , Bui, H.H., Xu, T. (2015). A laboratory-scale study of the aqueous mineral carbonation of coal fly ash for CO_2 sequestration, *Journal of Cleaner Production, 103*, 665-674. doi:10.1016/j.jclepro.2014.03.005

Zajac, M., Skibsted, J., Bullerjahn, F., Skocek, J. (2022). Semi-dry carbonation of recycled concrete paste, *Journal of CO_2 Utilization, 63*, 102111. doi:10.1016/j.jcou.2022.102111